SANDIA REPORT
SAND2021-10170
Printed August 2021

Sandia National Laboratories

Effects of Radiation Reaction Physics on High-Current Power Flow

Mark H. Hess and Evstati G. Evstatiev

Prepared by
Sandia National Laboratories
Albuquerque, New Mexico 87185
Livermore, California 94550

Issued by Sandia National Laboratories, operated for the United States Department of Energy by National Technology & Engineering Solutions of Sandia, LLC.

Available to DOE and DOE contractors from

U.S. Department of Energy
Office of Scientific and Technical Information
P.O. Box 62
Oak Ridge, TN 37831

Telephone: (865) 576-8401
Facsimile: (865) 576-5728
E-Mail: reports@osti.gov
Online ordering: http://www.osti.gov/scitech

Available to the public from

U.S. Department of Commerce
National Technical Information Service
5301 Shawnee Road
Alexandria, VA 22312

Telephone: (800) 553-6847
Facsimile: (703) 605-6900
E-Mail: orders@ntis.gov
Online order: https://classic.ntis.gov/help/order-methods

Effects of Radiation Reaction Physics on High-Current Power Flow

Mark H. Hess
Org. 1684
Sandia National Laboratories
P.O. Box 5800
Albuquerque, NM 87185-1186
mhess@sandia.gov

Evstati G. Evstatiev
Org. 1684
Sandia National Laboratories
P.O. Box 5800
Albuquerque, NM 87185-1186
egevsta@sandia.gov

SAND2021-10170

ABSTRACT

In this study, we examine the effects of the radiation reaction force on electrons in a radial magnetically insulated transmission line (MITL) near a load with peak currents of 60+ MA. More specifically, we study the differences in electron motion and kinetic energy with or without radiation reaction physics using a novel guiding center drift approach that incorporates $\mathbf{E} \times \mathbf{B}$ and ∇B drifts. A key finding of this study is that an electron's magnetic moment, which would be conserved when radiation reaction physics is not incorporated, can be significantly reduced in magnetic fields on the order of 10,000's T when radiation reaction is included. The reduction of magnetic moment gives rise to a significant reduction in cycloidal kinetic energy as well as a reduction in the electron's ∇B drift.

ACKNOWLEDGMENT

Special thanks to Kristian Beckwith for helpful comments on this study.

CONTENTS

LIST OF FIGURES

SUMMARY

In this study, we model radiation reaction physics on electron motion in a 60+ MA radial MITL using a drift kinetic approach that incorporates $\mathbf{E} \times \mathbf{B}$ and ∇B drifts. The magnitudes of the peak current, electric field, and magnetic field in the radial MITL used this study are comparable to those found in designs of NGPP machines at Sandia National Laboratories. Turning radiation reaction physics on/off is accomplished by making the electron's magnetic moment time-dependent/conserved. The study demonstrates that the electron's magnetic moment, cycloidal kinetic energy, and ∇B drift can be significantly affected when the electron experiences a magnetic field with a magnitude $> 10,000$ T within the radial MITL.

NOMENCLATURE

electric field one component of an electromagnetic vector field, or light, which applies a force to a charged particle in the same direction as the electric field component

E $\times$ B drift a guiding center drift motion that results in the presence of combined electric and magnetic fields

∇B **or grad** B **drift** a guiding center drift motion that results in a non-uniform magnetic field

guiding center drift kinetics a method for describing a charged particle's average drift motion without resolving the rapidly varying cycloidal orbit which occurs in the presence of a magnetic field

load the inner most section of the MITL which results in the highest magnetic field

Lorentz Force Law a description of forces that a charged particle, such as an electron, experiences in electric and magnetic fields

Lorentz-Abraham-Dirac Force Law a relativistic description of forces that a charged particle experiences which includes the radiation reaction force

magnetic field one component of an electromagnetic vector field, or light, which applies a force to a charged particle in a direction perpendicular to the particle's velocity and the magnetic field component

magnetic moment a measure of a particle's cycloidal kinetic energy per magnetic field and an adiabatic invariant of a particle's motion (when radiation reaction is absent)

MITL also known as a magnetically insulated transmission line, is a section of a pulsed power machine which delivers electrical power and high-magnetic fields to a load

NGPP also known as Next Generation Pulsed Power, is a machine being designed at Sandia National Laboratories which can deliver 60+ MA of current to a load

pulse length the characteristic time over which the current in a MITL is ramped to its peak value

peak current the maximum current achieved by the MITL

radiation the emission of particles (in this study just photons) by another particle

radiation reaction force a force on a particle that results from the emission of radiation

synchrotron radiation a type of radiation that is emitted by charged particles, such as electrons, when accelerated by the presence of a magnetic field

1. CHAPTER 1: THEORY

1.1. Radiation and the Radiation Reaction Force: A Brief History

Radiation physics and its corresponding radiation reaction force physics has had a long history which we will briefly highlight. J. J. Larmor predicted that accelerating charges would emit radiation in 1897 [1]. This prediction was improved with the incorporation of relativistic physics in 1898 by A. -M. Liénard using what are now known as the Liénard-Wiechert potentials [2]. In 1899, H. A. Lorentz developed a charged particle force law, known as the Lorentz Force Law, for particles in electric and magnetic fields [3]. And in 1902, M. Abraham considered a radiation reaction force term to account for the emission of radiation by accelerating charges that was predicted by J. J. Larmor [4]. This new force law became known as the Lorentz-Abraham Force Law. Decades later in 1938, P. A. M. Dirac formulated a relativistic covariant version of the force law which was consistent with the relativistic radiation formula predicted by A. -M. Lienard [5]. The fully relativistic force law became known as the Lorentz-Abraham-Dirac Law. In 1947, radiation from electrons bending in a magnetic field, now known as "synchrotron radiation", was experimentally measured by F. R. Elder and collaborators on a General Electric synchrotron [6]. Two years later, J. Schwinger published a definitive analysis of the properties of synchrotron radiation [7]. Over the next 70 years, numerous works on radiation reaction physics for charged particles accelerating in electric and magnetic fields have been published.

1.2. Lorentz-Abraham-Dirac Force Law

The Lorentz-Abraham-Dirac [8, 9] force law describes the motion of a relativistic charged particle in electric and magnetic fields and includes the effect of radiation, e.g. synchrotron radiation, by the particle. The force law includes the standard Lorentz force law term and a radiation reaction force term

$$\frac{d\mathbf{p}}{dt} = \mathbf{F} + \mathbf{F}_{rad} \tag{1}$$

where the Lorentz force law is given by

$$\mathbf{F} = q(\mathbf{E} + \mathbf{v} \times \mathbf{B}). \tag{2}$$

The radiation reaction force can be computed from both the particle's motion as well as the Lorentz force and is given by,

$$\mathbf{F}_{rad} = \tau(\gamma\frac{d\mathbf{F}}{dt} - \frac{\gamma^3}{c^2}(\frac{d\mathbf{v}}{dt} \times (\mathbf{v} \times \mathbf{F}))), \tag{3}$$

where τ is a characteristic time scale for electrons given by

$$\tau = \frac{e^2}{6\pi\varepsilon_0 mc^2} = 6.3 \text{ x } 10^{-24}\text{s}. \tag{4}$$

It is instructive to consider the radiation reaction force for a Lorentz force corresponding to a uniform magnetic field $\mathbf{B} = B\mathbf{e}_y$ with no electric field is present. Although this case is simplistic,

it uncovers the most important contribution to the radiation reaction force. We assume that the particle has its velocity and momenta in all three directions, i.e. $\mathbf{v} = v_x\mathbf{e}_x + v_y\mathbf{e}_y + v_z\mathbf{e}_z$ and $\mathbf{p} = p_x\mathbf{e}_x + p_y\mathbf{e}_y + p_z\mathbf{e}_z$. The radiation reaction force can be computed from Eq. (3) and its calculation is shown in Appendix A. The radiation reaction force is given by

$$\mathbf{F}_{rad} = -\frac{\gamma v_\perp^2/c^2\mathbf{p}_\parallel}{\tau_{damp}} - \frac{\gamma(1-v_\parallel^2/c^2)\mathbf{p}_\perp}{\tau_{damp}}. \tag{5}$$

In Eq. (5), we define $\mathbf{v}_\parallel = v_y\mathbf{e}_y$, $\mathbf{p}_\parallel = p_y\mathbf{e}_y$, $\mathbf{v}_\perp = v_x\mathbf{e}_x + v_z\mathbf{e}_z$, $\mathbf{p}_\perp = p_x\mathbf{e}_x + p_z\mathbf{e}_z$, $\gamma = 1/\sqrt{1-v^2/c^2} = \sqrt{1+p^2/m^2c^2}$ is the relativistic factor, and the characteristic damping time is given by

$$\tau_{damp} = \frac{m^2}{q^2B^2\tau}. \tag{6}$$

Fig. 1-1 shows a log-log plot of τ_{damp}. We expect that the radiation reaction force is important when τ_{damp} is equal to or less than a characteristic time scale in the system.

At Sandia National Laboratories, we are in the process of designing a Next Generation Pulsed Power (NGPP) machine [10], which at 60+ MA peak currents will produce magnetic fields in excess of 100,000 T near the load. Electrons in the extreme magnetic fields of this pulsed power facility are expected to produce synchrotron radiation and be affected by the radiation reaction force. One important time scale for a NGPP machine design is the pulse length τ_{pulse}. In the present study, we focus our attention on NGPP current pulse lengths of 100 ns and 200 ns. In these cases, τ_{damp} is equal to or less than 100 ns when B $>$ 7200 T and τ_{damp} is equal to or less than 200 ns when B $>$ 5100 T. Fig. 1-1 shows a current pulse length region in blue and a region where $\tau_{damp} < \tau_{pulse}$ in red.

Consider now the case where the electron is in uniform electric and magnetic fields $\mathbf{E} = E\mathbf{e}_x$ $\mathbf{B} = B\mathbf{e}_y$, respectively. By transforming to the $\mathbf{E}\times\mathbf{B}$ guiding center drift frame velocity [11], i.e.

$$\mathbf{V}_{gc} = \frac{\mathbf{E}\times\mathbf{B}}{B^2}, \tag{7}$$

the electric field in the new frame is zero and the magnetic field is given by $B' = B\sqrt{1-E^2/B^2c^2}$. We should note that for practical application to high-power MITLs the $\mathbf{E}\times\mathbf{B}$ drift velocity is non-relativistic, in which case $B' = B$ and $t' = t$. We will make this assumption for the remainder of the report. In the transformed frame, the radiation reaction force will be identical to Eq. (5). Hence the particle's cycloidal momentum, and corresponding kinetic energy, will be damped. By transforming back to the laboratory frame, the particle's entire motion will consist of the uniform $\mathbf{E}\times\mathbf{B}$ drift Eq. (7) and a damped cycloidal motion. From this calculation, we can see that the $\mathbf{E}\times\mathbf{B}$ drift is left unaffected by the radiation reaction force.

The magnitude of the radiation reaction force due to other types of drift motion is typically much smaller than Eq. (5). For example as is well-known in inner MITL systems, we expect that the particle will undergo ∇B drift due to the spatially varying magnetic field in the MITL. Since the average magnitude of the Lorentz force is $|qv_\perp B|$, then we expect that the Lorentz force perturbation due to the spatially varying magnetic field will have a magnitude on the order $|qv_\perp r_L\nabla B|$ where $r_L = |p/qB|$ is the relativistic Larmor radius. In general, $|r_L\nabla B/B| << 1$ for

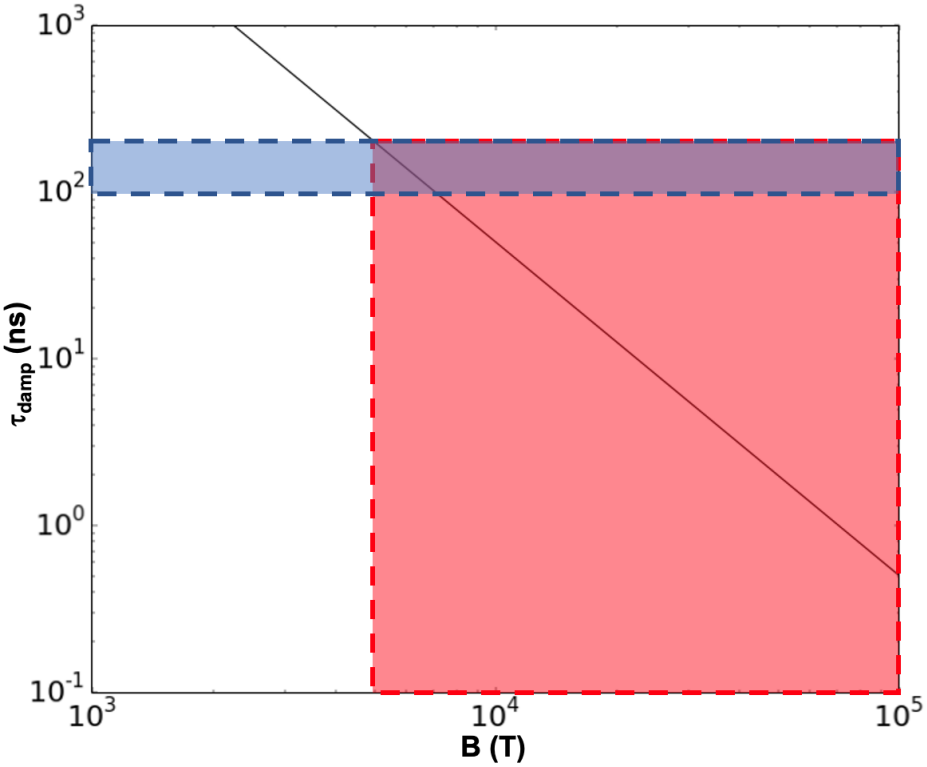

Figure 1-1 Log-log plot of τ_{damp} (ns) as a function of the magnetic field (T) with 100-200 ns possible NGPP pulse length region (blue) and the τ_{damp} less than the current pulse length region (red).

MITL systems, and hence the additional radiation reaction terms are small compared to Eq. (5). For the remainder of this report, we will assume that the radiation reaction force is given by Eq. (5).

1.3. Radial MITL: Geometry, Fields, and Equations of Motion

The geometry for the cylindrically symmetric radial MITL that we are considering for this study is shown in Fig. 1-2. The key elements of this geometry in cylindrical coordinates are anode and cathode planes denoted by $z = z_a$ and $z = z_c$ respectively, and an axial load denoted by $r = r_l$. All surfaces of the MITL are assumed to be perfect conductors.

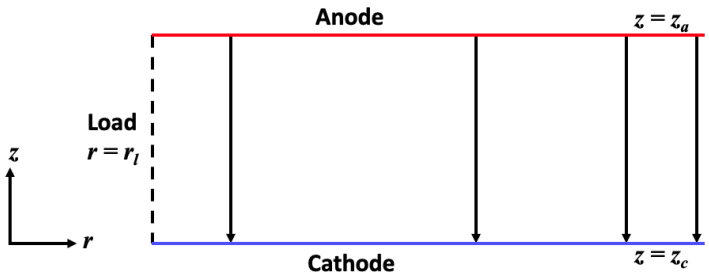

Figure 1-2 Schematic of the radial MITL showing the anode, cathode, load, axis of symmetry at $r = 0$, and the direction of the electric field lines (arrows).

The electric and magnetic vacuum fields in this system can be described to an excellent manner with the speed of light approaches infinity approximation, i.e. $c \to \infty$, as shown in recent work by Hess and Evstatiev [12]. The fields were found to be

$$\mathbf{E} = -\frac{\mu_0 \dot{I}}{2\pi} \ln\left(\frac{r}{r_l}\right) \mathbf{e}_z, \tag{8}$$

and

$$\mathbf{B} = -\frac{\mu_0 I(t) \mathbf{e}_\phi}{2\pi r}, \tag{9}$$

where $I(t)$ is the time-dependent current in the MITL, $\dot{I} = dI/dt$ is the time derivative of the current, and $\mathbf{e}_z$ and $\mathbf{e}_\phi$ are the unit vectors in the positive z and ϕ directions respectively. An excellent current model for the existing Z-Machine as well as a NGPP machine is a sine-squared profile given by,

$$I(t) = I_{peak} \sin^2\left(\frac{\pi t}{2\tau_{pulse}}\right), \tag{10}$$

where I_{peak} is the peak current and τ_{pulse} is the characteristic current pulse length. In this study, we assume that the NGPP machine has three possible peak currents given by I_{peak} = 60 MA, 70 MA, and 80 MA and two possible current pulse lengths given by τ_{pulse} = 100 ns and 200 ns.

1.4. Motion of an Electron in a Radial MITL

In order to derive the full equations of motion in the radial MITL geometry, we start with the momentum equation using the Lorentz force law, i.e.

$$\frac{d\mathbf{p}}{dt} = q(\mathbf{E} + \mathbf{v} \times \mathbf{B}) \tag{11}$$

where $\mathbf{p} = \gamma m \mathbf{v}$ is the particle's relativistic momentum, $\mathbf{v}$ is the particle's velocity, and $\gamma = 1/\sqrt{1 - v^2/c^2}$ is the relativistic factor with $v^2 = v_r^2 + v_\phi^2 + v_z^2$. It is useful to note that γ can also be expressed in terms of the momentum as $\gamma = \sqrt{1 + p^2/m^2c^2}$ where $p^2 = p_r^2 + p_\phi^2 + p_z^2$. The momenta equations for all components are given by

$$\frac{dp_r}{dt} = \frac{p_\phi^2}{\gamma m r} + \frac{q\mu_0 I v_z}{2\pi r} + \mathbf{F}_{rad,r} \cdot \mathbf{e}_r, \tag{12}$$

$$\frac{dp_\phi}{dt} = -\frac{p_r p_\phi}{\gamma m r} + \mathbf{F}_{rad,\phi} \cdot \mathbf{e}_\phi, \tag{13}$$

$$\frac{dp_z}{dt} = -\frac{q\mu_0}{2\pi}\frac{dI}{dt}\ln\left(\frac{r}{r_l}\right) - \frac{q\mu_0 I v_r}{2\pi r} + \mathbf{F}_{rad,z} \cdot \mathbf{e}_z, \tag{14}$$

where the radiation reaction force is given by Eq. (5) and the parallel direction is in the $\mathbf{e}_\phi$ direction. The position of the particle can be found from

$$\frac{dr}{dt} = v_r, \quad \frac{d\phi}{dt} = \frac{v_\phi}{r}, \quad \frac{dz}{dt} = v_z. \tag{15}$$

Since the only motion in the phi direction is due to emission at a MITL surface, e.g. 1 eV thermal emission, we will assume for the remainder of this report that the $v_\phi = 0$ and $\mathbf{p}_\phi = 0$. The reduced momenta equations are given by

$$\frac{dp_r}{dt} = \frac{q\mu_0 I v_z}{2\pi r} + \mathbf{F}_{rad,r} \cdot \mathbf{e}_r, \tag{16}$$

$$\frac{dp_\phi}{dt} = 0, \tag{17}$$

$$\frac{dp_z}{dt} = \ln\left(\frac{r}{r_l}\right) - \frac{q\mu_0 I v_r}{2\pi r} + \mathbf{F}_{rad,z} \cdot \mathbf{e}_z. \tag{18}$$

Recent work by Hess and Evstatiev [12] have shown that when the radiation reaction is not considered, the electron motion in a MITL can be successfully described using a combined $\mathbf{E} \times \mathbf{B}$ and ∇B drift description for the a given $\mathbf{E}$ and $\mathbf{B}$ within the MITL. More specifically, the guiding center velocity [11, 13, 14, 15, 16, 17] is described as

$$\mathbf{V}_{gc} = \frac{\mathbf{E} \times \mathbf{B}}{B^2} + \frac{\mu}{q\gamma}\frac{\mathbf{B} \times \nabla B}{B^2}, \tag{19}$$

where μ is the adiabatic invariant. The adiabatic invariant, which is equivalent to the particle's magnetic moment, is given by

$$\mu = \frac{p_{r,\mathrm{osc}}^2 + p_{z,\mathrm{osc}}^2}{2mB}, \tag{20}$$

Since the magnetic moment is proportional to cycloidal kinetic energy, this quantity will be damped by the radiation reaction force. Therefore, the magnetic moment is given by $\mu(t)$, and we will assume for the remainder of this report that the guiding center velocity of the particle is given by

$$\mathbf{V}_{gc} = \frac{\mathbf{E}\times\mathbf{B}}{B^2} + \frac{\mu(t)}{q\gamma}\frac{\mathbf{B}\times\nabla B}{B^2}. \tag{21}$$

1.5. Physics Modeling in a Radial MITL

Although the reduced equations of motion for a particle in a radial MITL (in the $c\to\infty$ limit) are given by Eqs. (16), (17), and (18), these equations are in general too challenging to solve since they require very small time scales in order to resolve cyclotron orbits. Instead, we are only interested in the guiding center motion of the particle along with the change in kinetic energy of the particle. The guiding center motion is given by Eq. (21) from the previous section, and it requires tracking of the time-dependent magnetic moment. As we will now show, the cycloidal momentum and kinetic energy can both be derived from the magnetic moment. From Eq. (20), we find that the magnitude of the relativistic cycloidal momentum and cycloidal kinetic energy can be written as

$$p_{cyc} = \sqrt{2\mu m B} \tag{22}$$

and

$$K_{cyc} = (\sqrt{1+2\mu B/mc^2}-1)mc^2. \tag{23}$$

The damping of the magnetic moment due to radiation reaction can be computed from

$$\frac{d\mu}{dt} = \frac{2\mu}{p_{cyc}}\frac{dp_{cyc}}{dt}|_{rad} = \frac{2\mu}{p_{cyc}}F_{rad}. \tag{24}$$

Using Eq. (5) along with the assumption $v_{\|} = v_{\phi} = 0$ yields the following damping equation for the magnetic moment,

$$\frac{d\mu}{dt} = -\frac{2\mu\tau q^2 B^2}{m^2}\sqrt{1+2\mu B/mc^2} = -\frac{2\mu}{\tau_{damp}}\sqrt{1+2\mu B/mc^2}. \tag{25}$$

Therefore, the guiding center drift velocity equation given by Eq. (21), the time-dependent magnetic moment equation given by Eq. (25), and the cycloidal kinetic energy equation given by Eq. (23), provide a complete description of a particle's guiding center motion and its cycloidal kinetic energy with the presence of radiation reaction. The total energy which is a combination of the cycloidal kinetic energy and the guiding center drift kinetic energy is given by

$$K_{tot} = K_{cyc} + \frac{1}{2}mV_{gc}^2. \tag{26}$$

For the remainder of this report, we will focus our attention on the total kinetic energy as a function of time shown in Eq. (26), but the cycloidal kinetic energy can be readily computed using Eq. (23).

It is useful to point out that radiation reaction physics in the previous equations can be turned off by setting $\tau = 0$ or equivalently $\tau_{damp}\to\infty$. When radiation reaction physics is turned off, then the magnetic moment is conserved as shown in Eq. (25).

2. CHAPTER 2: COMPARATIVE MITL SIMULATIONS WITH AND WITHOUT RADIATION REACTION

2.1. Simulation Description

In this LDRD study, we look at the effects of radiation reaction physics on electrons for peak currents, current pulse lengths, and load radii that are in the regime of interest for a NGPP radial MITL. In particular, we look at NGPP parameters corresponding to I_{peak} = 60 MA, 70 MA, and 80 MA, τ_{pulse} = 100 ns and 200 ns, and r_l = 100 μm and 1 mm. In all cases, we made the assumption that the MITL gap width is 1 cm. As a comparison, existing MagLIF experiments have approximately 20 MA peak currents with current pulse lengths of approximately 120 ns that produce stagnation columns which can be less than 100 μm [18].

The simulations performed in this study are separated into two categories. The first category examined electron motion assuming that the electrons were emitted from the cathode when the local electric field first reaches the critical threshold $E_{th} = 24MV/m$ [19]. Under this condition, the electron's initial magnetic moment is given by $\mu = 2E^2/mB^3 = 2E_{th}^2/mB^3$ which was found in previously cited MITL work by Hess and Evstatiev. In these simulations, the electrons are emitted at different radial locations with respect to the load, i.e. $10 \times r_l$, $9 \times r_l$ $8 \times r_l$, $7 \times r_l$, $6 \times r_l$, $5 \times r_l$, and $4 \times r_l$. We should note that the electric field threshold can first occur early in the current pulse, if the particle is sufficiently far from the load.

The second category of simulations explores what happens when the electrons are emitted at later times with respect to the current pulse, e.g. emission times when the current is 5%, 10%, 25%, and 50% of the peak current. In these simulations, we also assume that the initial magnetic moment is $\mu = 2E^2/mB^3 = 2E_{th}^2/mB^3$. This assumption would correspond to an emission model in which the local electric field has been limited to the critical threshold value due to space-charge physics. Again the electrons are emitted at different radial locations relative to the load. Fig. 2-1 summarizes the parameter changes for the simulations performed in this study.

Simulation Category	Peak Current (MA)	Pulse Length (ns)	Load Radius (mm)	Electron Emission Time
First	60, 70, 80	100, 200	0.1, 1.0	$E=E_{th}$
Second	60, 70, 80	100, 200	0.1, 1.0	I = 5%, 10%, 25%, 50% peak current

Figure 2-1 Table showing the types of simulations performed in this study.

As is shown in the table, the entire study analyzes the effects of radiation reaction while varying a number of different parameters that are relevant to NGPP. In the following sections, we only summarize the findings of a subset of this study. The simulation output for all of these parameter studies is available upon request.

2.2. Electron simulations on a 60 MA / 100 ns NGPP with a 100 μm load

We start our discussion of the simulation study, with the case of I_{peak} = 60 MA, r_l = 100 microns, and τ_{pulse} = 100 ns. Again we make the assumption that electrons are emitted when the vacuum electric field first reaches the critical threshold of $E_{th} = 24MV/m$. The gap width and the height of the load are fixed at 1 cm. Electrons are initiated at different cathode radii with respect to the load radius, and the electron's motion is tracked using Eq. (21). Its magnetic moment is found using Eq. (25), and its cycloidal and total kinetic energies are found from Eqs. (23) and (26), respectively. In these simulations, we compare electron motion and kinetic energy with and without radiation reaction physics. As we mentioned previously, when radiation reaction is turned off, e.g. by setting $\tau = 0$ or equivalently $\tau_{damp} \to \infty$, then the electron's magnetic moment, μ, is conserved. However, when radiation reaction physics is turned on, then the magnetic moment is time-dependent, which results in a reduction in the electron's kinetic energy and a change in its ∇B drift.

In the following plots, curves that are solid denote radiation reaction physics turned off, and curves that are dashed denote radiation reaction turned on. Moreover, the color coding on the solid curves denotes the initial conditions for the electron relative to the load, i.e. $10 \times r_l$ (blue), $9 \times r_l$ (green), $8 \times r_l$ (red), $7 \times r_l$ (cyan), $6 \times r_l$ (magenta), $5 \times r_l$ (yellow), and $4 \times r_l$ (black). Fig. 2-2 shows a plot of the electron's magnetic moment as a function of time. Notice that each of the solid curves, which correspond to radiation reaction physics turned off, are constants since the magnetic moment is an adiabatically conserved quantity. However for each solid curve, we see a dashed curve corresponding to the same electron initial condition, which is significantly decreasing as a function of time. This implies that the electron's kinetic energy and its ∇B drift will be different than the case without radiation reaction.

Although the electron's magnetic moment is decreasing as a function of time, it is instructive to see how the electron's moment is decreasing as a function of the magnetic field that it's experiencing. Fig. 2-3 shows a plot of the magnetic moment versus the magnetic field. It is apparent that the electron is experiencing a much larger magnetic field later in time compared to its initial magnetic field. The reason for this is that the electron's radial position is decreasing due to $\mathbf{E} \times \mathbf{B}$ drift while the current is simultaneously increasing. Notice that the electron is experiencing magnetic field strengths of around 120,000 T. This is due to the fact that the electron's radial position from the $\mathbf{E} \times \mathbf{B}$ drift is very close to the load at r_l = 100 microns and the current reaches a peak of 60 MA. The magnetic field strength at a radius of 100 μm and a current of 60 MA is 120,000 T. Also notice that the electron's magnetic moment is noticeably decreasing when the magnetic field is approximately 10,000 T. This is consistent with our previous explanation that $\tau_{damp} < \tau_{pulse}$ corresponds to 7,200 T for τ_{pulse} = 100 ns.

Since the total kinetic energy is related to the magnetic moment from Eqs. (23) and (26), then we expect that electron's kinetic energy will be different between cases with or without radiation reaction physics. Indeed, as shown in Fig. 2-4, there are significant differences in the total kinetic energy. The first noticeable difference is that for the case with no radiation reaction, the overall kinetic energy continues to rise until τ_{pulse} = 100 ns, whereas the kinetic energy reaches a peak and decreases much earlier in time when radiation reaction is turned on. Without radiation reaction, the electron's cycloidal kinetic energy continues to increase until peak current at

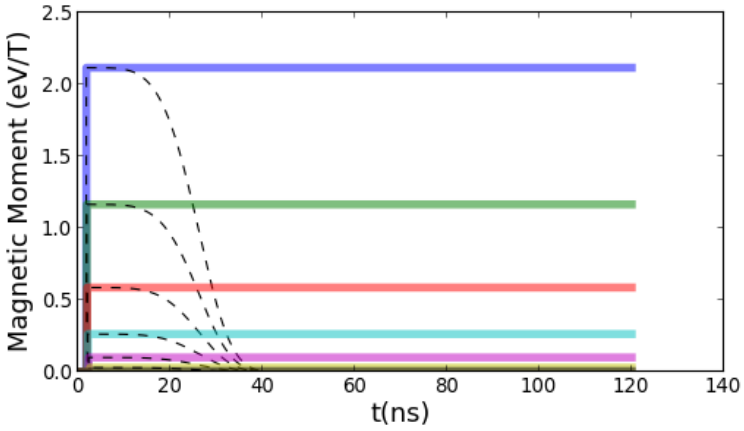

Figure 2-2 Plots of the magnetic moment of an electron versus time without radiation reaction (solid curves) and with radiation reaction (dashed curves) for I_{peak} = 60 MA, r_l = 100 μm, and τ_{pulse} = 100 ns. The solid curve colors denote different initial electron radii: 10 $\times$ r_l (blue), 9 $\times$ r_l (green), 8 $\times$ r_l (red), 7 $\times$ r_l (cyan), 6 $\times$ r_l (magenta), 5 $\times$ r_l (yellow), and 4 $\times$ r_l (black).

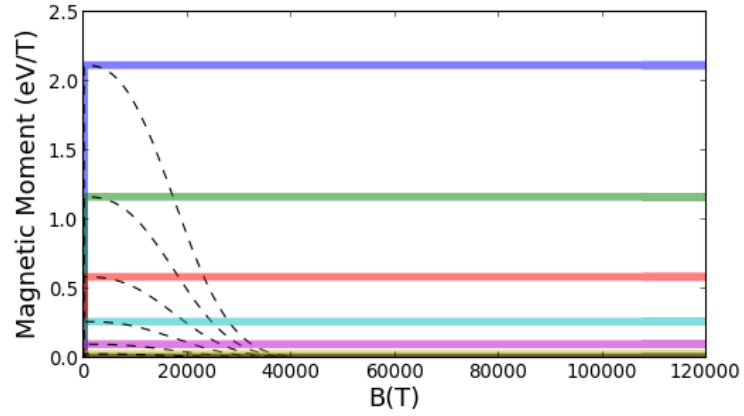

Figure 2-3 Plots of the magnetic moment of an electron versus magnetic field without radiation reaction (solid curves) and with radiation reaction (dashed curves) for I_{peak} = 60 MA, r_l = 100 μm, and τ_{pulse} = 100 ns.

$t = \tau_{pulse}$. We should note that the drift component of the total kinetic energy (second term in Eq. (26)) is negligible compared to the peak values of the cycloidal kinetic energy (first term in Eq. (26)). With radiation reaction, the cycloidal kinetic energy reaches a peak when

$$\frac{1}{\mu}\frac{d\mu}{dt} = -\frac{1}{B}\frac{dB}{dt}. \tag{27}$$

When the electron loses its magnetic moment it affects the cycloidal kinetic energy, and hence total kinetic energy, in two ways. First, the immediate loss of magnetic moment corresponds to an immediate loss of kinetic energy. Secondly, and possibly even more importantly, the electron loses its ability to gain more kinetic energy as the magnetic field grows, which is seen when the magnetic moment is conserved (no radiation reaction physics). The combination of the two effects, can lead to significant differences in the kinetic energy with and without radiation reaction as is illustrated in Fig. 2-4. The electron's drift motion is also affected by the decreasing magnetic

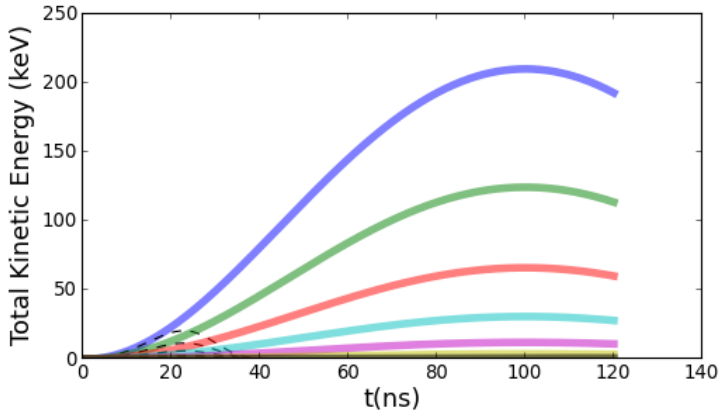

Figure 2-4 Plots of the total kinetic energy of an electron versus time without radiation reaction (solid curves) and with radiation reaction (dashed curves) for I_{peak} = 60 MA, r_l = 100 μm, and τ_{pulse} = 100 ns.

moment of the electron. Since the ∇B drift is proportional to the magnetic moment, then we expect that the electron's drift in the axial direction will be affected due to the decrease in magnetic moment. Fig. 2-5 shows a plot of electron trajectories near the load. When the magnetic moment is conserved without radiation reaction physics, then the electron axially deflects towards the anode as it approaches the load. However, when radiation reaction is turned on and the magnetic moment rapidly decreases, then we see that the electron's axial drift motion can be strongly reduced near the load. The result of this reduction in the electron's axial velocity is that the electron's axial position can have significant differences, e.g. mm-scale differences.

2.3. Electron simulations on a 60 MA /100 ns NGPP with a 1mm load

We now examine how the effect on radiation reaction when the load radius is increased by a factor of 10 to r_l = 1 mm. Since the peak magnetic field that the electron experiences is inversely proportional to r_l, then we expect that electrons will at most experience 12,000 T magnetic fields

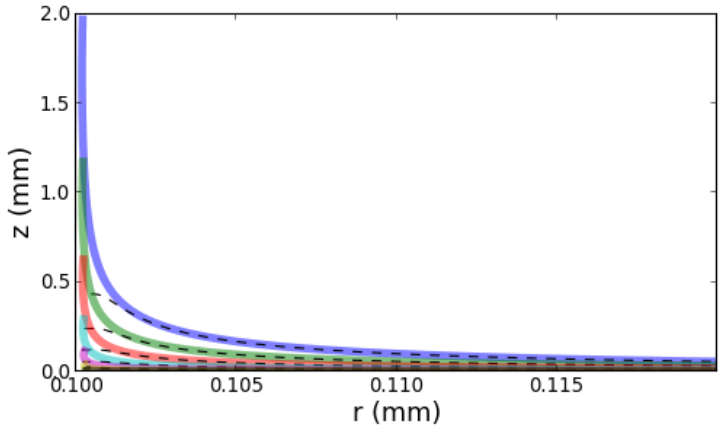

Figure 2-5 Plots of the electron guiding center motion without radiation reaction (solid curves) and with radiation reaction (dashed curves) for I_{peak} = 60 MA, r_l = 100 μm, and τ_{pulse} = 100 ns.

(1/10th of the 120,000 T in the previous example). This is indeed the case, and in general the magnetic field that the particle experiences can be significantly smaller than the previous example with r_l = 100 μm. Additionally, since we are initializing the electrons with a multiplicative factor with respect to the load radius, then the initial electric fields are larger and initial magnetic fields are smaller compared to the previous example. This implies that the initial magnetic moment $\mu = 2E_{th}^2/mB^3$ of each electron is significantly larger (by nearly three orders of magnitude) than in the previous case.

Fig. 2-6 shows the magnetic moment as a function of time for r_l = 1 mm case. Notice that for some of the particles, e.g. 10 $\times$ r_l case in blue, the magnetic moment is only plotted for a short time. For these these electrons, the magnetic moment is large enough that the ∇B drift causes the electron to intercept the anode before the end of the current pulse. When the electron intercepts the anode, we end the simulation. Electrons that are emitted sufficiently close to the load, e.g. the 6 $\times$ r_l case in magenta, have a magnetic moment small enough such that the particle does not intercept the anode during the current pulse and reach radii that are close to the load. In Fig. 2-7, one can see that the peak magnetic field that an electron experiences is around 12,000 T. One can also see in the magnified plot in Fig. 2-8 that the magnetic moment has a significant decrease when the magnetic field is around 7,000 T for the 7 $\times$ r_l case in cyan. This is consistent with our previous discussion that radiation reaction physics becomes important when $\tau_{damp} \leq \tau_{pulse}$.

From Fig. 2-9, one can immediately see that for electrons which experience higher magnetic fields near the load, e.g. 6 $\times$ r_l case, significant differences between the kinetic energy with and without radiation reaction may occur due to the loss of magnetic moment. One can also see that the loss of magnetic moment can lead to mm-scale differences in the axial position of the electron with and without radiation reaction as is shown in Fig. 2-10.

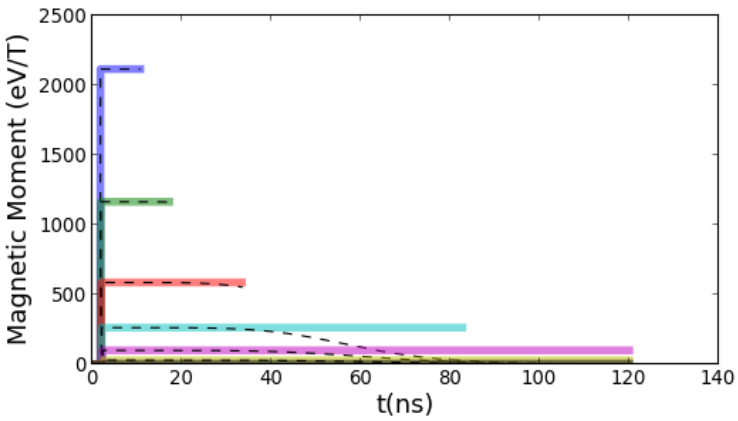

Figure 2-6 Plots of the magnetic moment of an electron versus time without radiation reaction (solid curves) and with radiation reaction (dashed curves) for I_{peak} = 60 MA, r_l = 1 mm, and τ_{pulse} = 100 ns. The solid curve colors denote different initial electron radii: 10 $\times$ r_l (blue), 9$\times$ r_l (green), 8 $\times$ r_l (red), 7 $\times$ r_l (cyan), 6 $\times$ r_l (magenta), 5 $\times$ r_l (yellow), and 4 $\times$ r_l (black).

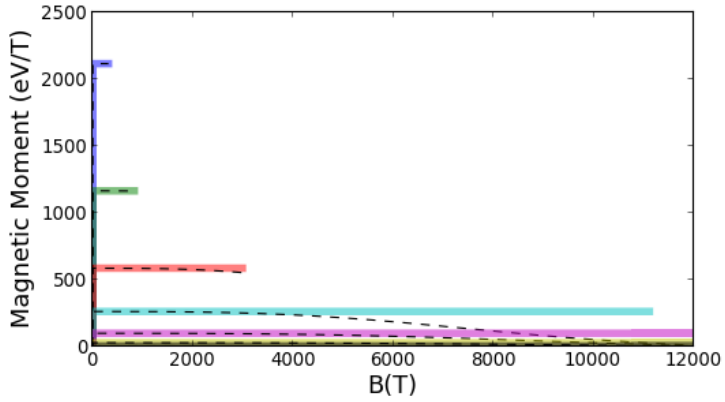

Figure 2-7 Plots of the magnetic moment of an electron versus magnetic field without radiation reaction (solid curves) and with radiation reaction (dashed curves) for I_{peak} = 60 MA, r_l = 1 mm, and τ_{pulse} = 100 ns.

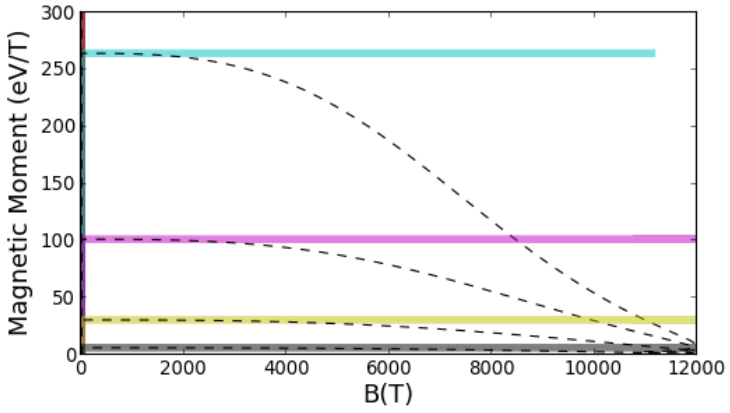

Figure 2-8 A magnified plot of the magnetic moment of an electron versus magnetic field without radiation reaction (solid curves) and with radiation reaction (dashed curves) for I_{peak} = 60 MA, r_l = 1 mm, and τ_{pulse} = 100 ns.

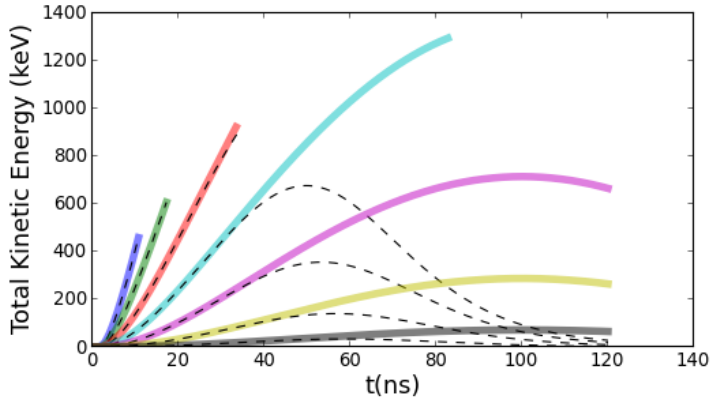

Figure 2-9 Plots of the total kinetic energy of an electron versus time without radiation reaction (solid curves) and with radiation reaction (dashed curves) for I_{peak} = 60 MA, r_l = 1 mm, and τ_{pulse} = 100 ns.

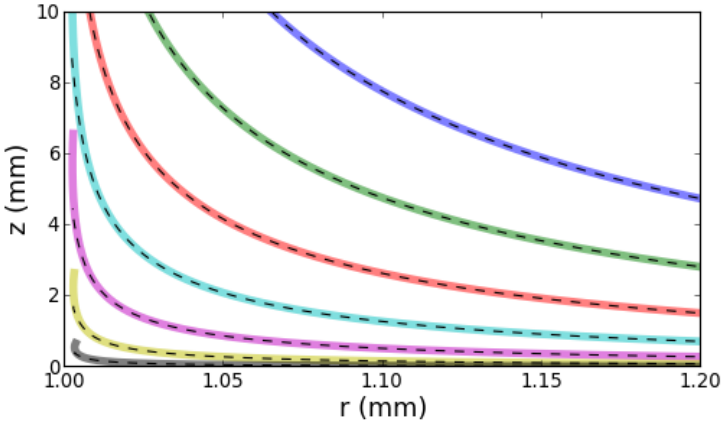

Figure 2-10 Plots of the electron guiding center motion without radiation reaction (solid curves) and with radiation reaction (dashed curves) for I_{peak} = 60 MA, r_l = 1 mm, and τ_{pulse} = 100 ns.

2.4. Electron simulations on a 60 MA /200 ns NGPP with a 100 μm load

We now look at how the current pulse length of a NGPP affects differences in electron simulations with and without radiation reaction physics. For these simulations, we assume that I_{peak} = 60 MA, r_l = 100 μm, and τ_{pulse} = 200 ns. Hence, the current pulse is now twice as long as the one considered in Section 2.1. From Fig. 1-1, we expect that radiation reaction physics will become important at even smaller magnetic fields for 200 ns pulse lengths, namely $B >$ 5,100 T, compared to the $B >$ 7,200 T for 100 ns. Indeed, this is the case. Figs. 2-11 and 2-12 show the decrease in magnetic moment as a function of time and magnetic field. Even though the magnetic moment temporally decreases on a time-scale twice as long as in the τ_{pulse} = 100 ns shown in Figs. 2-2, the decrease in magnetic moment as a function of magnetic field is even faster when comparing Figs. 2-12 and 2-3.

We should note that in these simulations the overall size of the magnetic moment for electrons in the τ_{pulse} = 200 ns is decreased by roughly 2 orders of magnitude compared to the τ_{pulse} = 200 ns case. The reason for this is that since dI/dt is lowered by a factor of two due to the doubling of the current pulse length, there is a time delay by which the electrons are emitted in these simulations. When the electrons are emitted in the τ_{pulse} = 200 ns case, the B-field has increased significantly compared to the τ_{pulse} = 100 ns case resulting in a lower magnetic moment. For example, the 10 x r_l electron is emitted at roughly t=1.8 ns when the magnetic field is 9.2 T for the τ_{pulse} = 100 ns case compared to emission at t=7.1 ns when the magnetic field is 37 T for the τ_{pulse} = 200 ns case.

The pulse length also has an effect on the difference between the electron's peak kinetic energy with or without radiation reaction physics. By comparing Figs. 2-13 and 2-4, one can see that there is a noticeable difference in the ratio of the peak kinetic energies for the 10 $\times$ r_l case. For the τ_{pulse} = 100 ns case, the ratio of the peak kinetic energy with and without radiation reaction physics is about 10%. Whereas for the τ_{pulse} = 200 ns case, the ratio drops to roughly 6.5%. Since

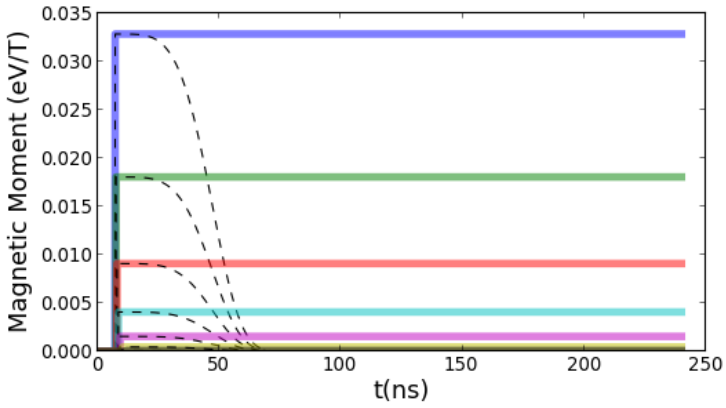

Figure 2-11 Plots of the magnetic moment of an electron versus time without radiation reaction (solid curves) and with radiation reaction (dashed curves) for I_{peak} = 60 MA, r_l = 100 μm, and τ_{pulse} = 200 ns. The solid curve colors denote different initial electron radii: 10 $\times$ r_l (blue), 9 $\times$ r_l (green), 8 $\times$ r_l (red), 7 $\times$ r_l (cyan), 6 $\times$ r_l (magenta), 5 $\times$ r_l (yellow), and 4 $\times$ r_l (black).

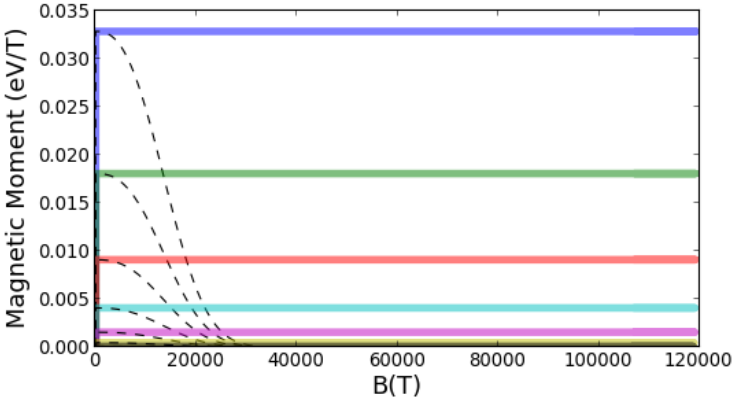

Figure 2-12 Plots of the magnetic moment of an electron versus magnetic field without radiation reaction (solid curves) and with radiation reaction (dashed curves) for I_{peak} = 60 MA, r_l = 100 μm, and τ_{pulse} = 200 ns.

the effect of radiation reaction physics can be seen at smaller magnetic fields for longer pulse lengths, the kinetic energy of the electron is reduced earlier relative to the pulse length.

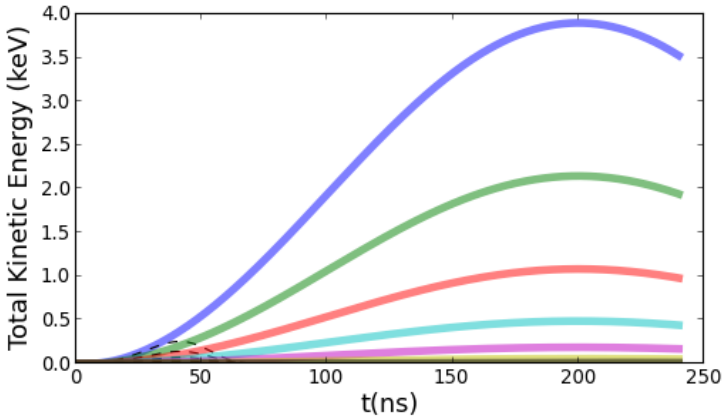

Figure 2-13 Plots of the total kinetic energy of an electron versus time without radiation reaction (solid curves) and with radiation reaction (dashed curves) for I_{peak} = 60 MA, r_l = 100 μm, and τ_{pulse} = 200 ns.

We end this section by looking at the electron guiding center trajectories. As is seen in previous trajectory plots, the rapid decrease of the magnetic moment causes the electron guiding center trajectory to have a reduced ∇B drift. Fig. 2-14 clearly illustrates this point. We should note that since the initial magnetic moment is much smaller for τ_{pulse} = 200 ns case compared to τ_{pulse} = 100 ns case, then the overall difference in the trajectories with and without radiation reaction physics is much smaller (10's μm compared to mm-scale).

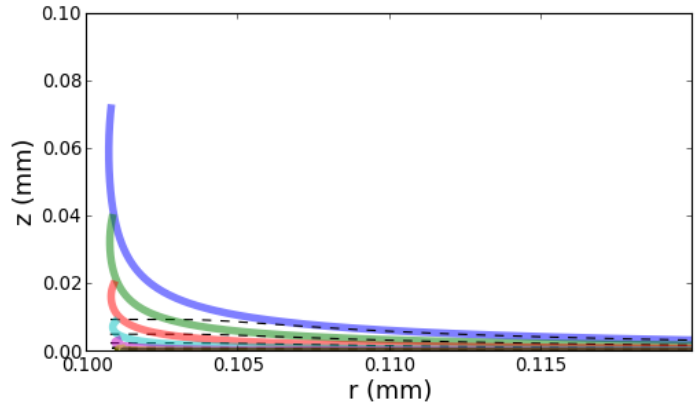

Figure 2-14 Plots of the electron guiding center motion without radiation reaction (solid curves) and with radiation reaction (dashed curves) for I_{peak} = 60 MA, r_l = 100 μm, and τ_{pulse} = 200 ns.

2.5. Electron simulations on a 80 MA /100 ns NGPP with a 100 μm load

Since there are designs of NGPP which have peak currents in the 80 MA range, in this section we expand our simulations to include the case I_{peak} = 80 MA, r_l = 100 μm, and τ_{pulse} = 100 ns. Obviously, since the peak current is now 33% higher than for the 60 MA case, we expect that the magnetic fields experienced by electrons will be increased by 33% as well. This implies that electrons will reach magnetic fields $\approx$ 7,200 T even earlier than in previous simulations. The result of this is that the magnetic moment, and hence kinetic energy, will be reduced even earlier in time than in the 60 MA case.

Fig. 2-15 shows a faster percentage decrease in the magnetic moment compared to the 60MA case shown in Fig. 2-2. Additionally, electrons can experience approximately 160,000 T near the load as shown in Fig. 2-16, which is 33% higher than in the 60 MA case. However, the electron's magnetic moment is largely decreased by the time the electron reaches 40,000 T which also occurred in Fig. 2-3.

The electron's kinetic energy and trajectories are significantly affected due to radiation reaction in similar ways as was shown in the 60 MA case. In particular, the peak kinetic energy with radiation reaction only reaches 10% of the peak without radiation reaction. Moreover, the loss of magnetic moment, and hence ∇B drift, causes mm-scale differences in the electron's axial position with and without radiation reaction.

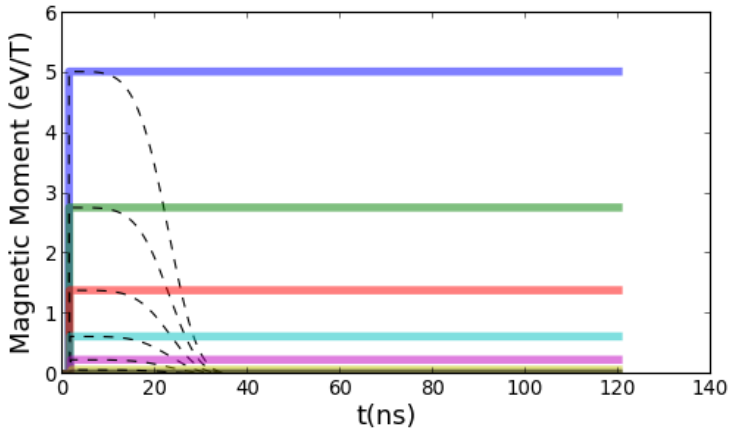

Figure 2-15 Plots of the magnetic moment of an electron versus time without radiation reaction (solid curves) and with radiation reaction (dashed curves) for I_{peak} = 80 MA, r_l = 100 μm, and τ_{pulse} = 100 ns. The solid curve colors denote different initial electron radii: 10 $\times$ r_l (blue), 9 $\times$ r_l (green), 8 $\times$ r_l (red), 7 $\times$ r_l (cyan), 6 $\times$ r_l (magenta), 5 $\times$ r_l (yellow), and 4 $\times$ r_l (black).

2.6. Electron simulations on a 60 MA /100 ns NGPP with a 100 μm load and emission at 5% peak current

As mentioned previously, we also examined the effects of radiation reaction when electrons are emitted later in time, e.g. emission times when the current is 5%, 10%, 25%, and 50% of the peak

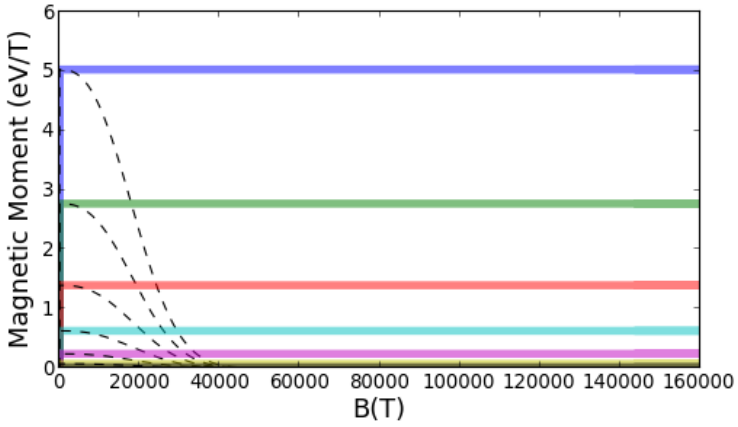

Figure 2-16 Plots of the magnetic moment of an electron versus magnetic field without radiation reaction (solid curves) and with radiation reaction (dashed curves) for I_{peak} = 80 MA, r_l = 100 μm, and τ_{pulse} = 100 ns.

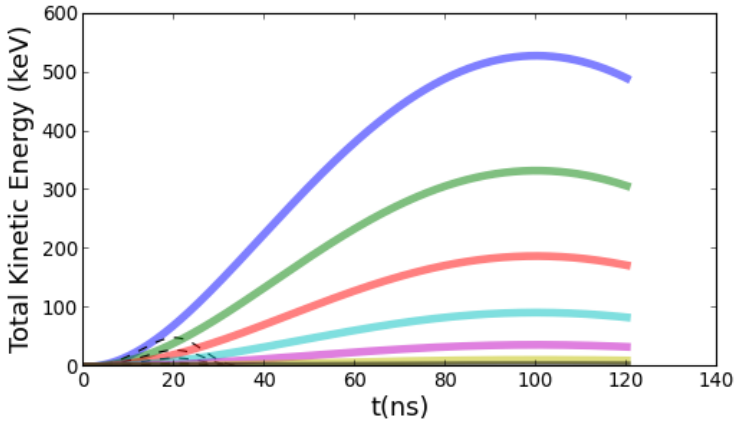

Figure 2-17 Plots of the total kinetic energy of an electron versus time without radiation reaction (solid curves) and with radiation reaction (dashed curves) for I_{peak} = 80 MA, r_l = 100 μm, and τ_{pulse} = 100 ns.

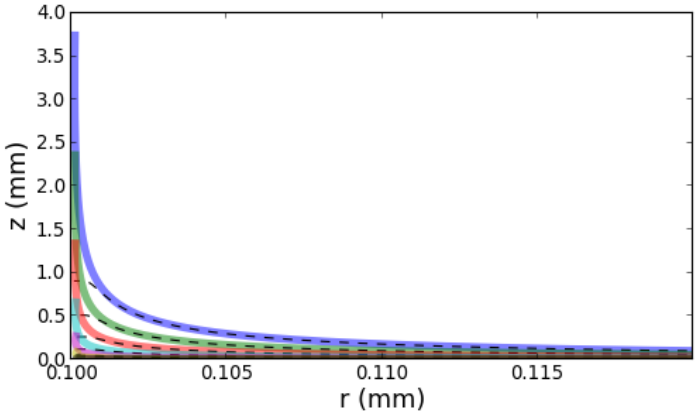

Figure 2-18 Plots of the electron guiding center motion without radiation reaction (solid curves) and with radiation reaction (dashed curves) for I_{peak} = 80 MA, r_l = 100 μm, and τ_{pulse} = 100 ns.

current. In this Section, we show the results of simulations when electron emission occurs at 5% of peak current. We make the assumption in these simulations that the initial value of the magnetic moment is given by $\mu = 2E_{th}^2/mB^3$. This corresponds to the assumption that space-charge fields due to the electrons already emitted from the cathode surface have maintained the electric field at the cathode surface to be E_{th}. It is quite possible that the space-charge electric field at the cathode surface computed in a fully electromagnetic manner results in an even lower value of the electric field than E_{th} resulting in lower values of the initial magnetic moment. One can therefore view these simulations as incorporating upper bound values of the magnetic moment when electrons are emitted at 5% peak current.

Since the current, and hence the magnitude of the magnetic field, is larger when the current is at 5% of the peak current compared to previous simulations with emission occurring when the electric field first reaches E_{th}, we expect that the initial magnetic moment is smaller than in previous simulations. This is clearly seen when comparing Figs. 2-19 and 2-2 where the initial magnetic moment is reduced by nearly 6 orders of magnitude. All of the radiation reaction effects that were discussed previously, i.e. loss of magnetic moment, loss of kinetic energy, and reduction of ∇B drift still apply to the present case. The only difference is that the absolute differences in kinetic energy and axial displacement between electrons with and without radiation reaction physics is significantly smaller by roughly 6 and 5 orders of magnitude, respectively.

For emission times that are later than 5% of the peak current, e.g. 10%, 25%, and 50% of the peak current, the magnetic field is even larger yielding even smaller initial magnetic moments. More specifically, the initial magnetic moments for emission at 10%, 25%, and 50% of the peak current cases, are 12.5 %, 0.8 %, and 0.1 % of those for emission at 5% of the peak current. Therefore the overall differences in kinetic energy and axial displacement between electron simulations with and without radiation reaction is reduced by these percentages, as well.

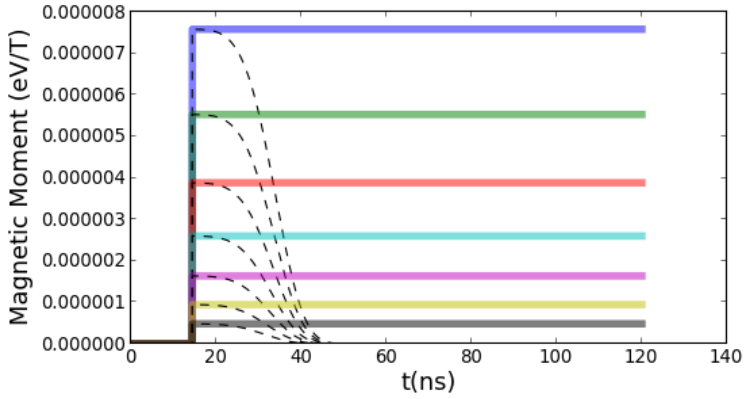

Figure 2-19 Plots of the magnetic moment of an electron versus time without radiation reaction (solid curves) and with radiation reaction (dashed curves) for I_{peak} = 60 MA, r_l = 100 μm, τ_{pulse} = 100 ns, and electron emission at 5% peak current. The solid curve colors denote different initial electron radii: 10 $\times$ r_l (blue), 9 $\times$ r_l (green), 8 $\times$ r_l (red), 7 $\times$ r_l (cyan), 6 $\times$ r_l (magenta), 5 $\times$ r_l (yellow), and 4 $\times$ r_l (black).

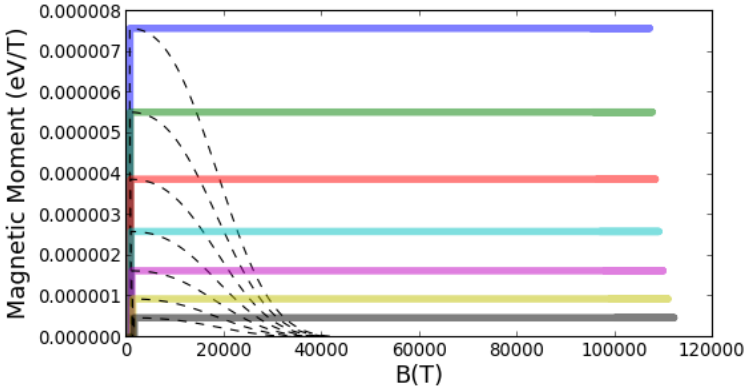

Figure 2-20 Plots of the magnetic moment of an electron versus magnetic field without radiation reaction (solid curves) and with radiation reaction (dashed curves) for I_{peak} = 60 MA, r_l = 100 μm, τ_{pulse} = 100 ns, and electron emission at 5% peak current.

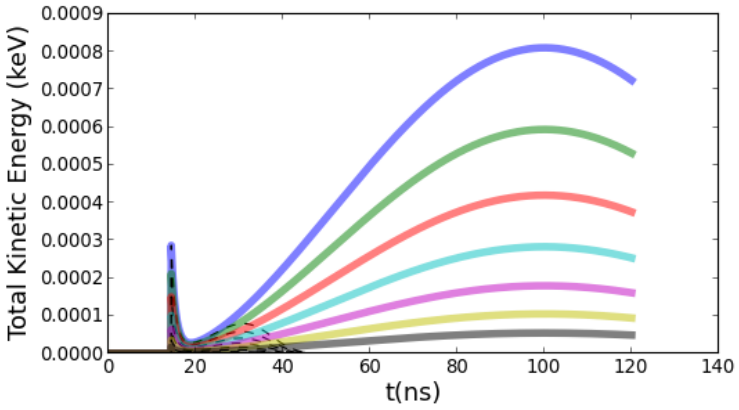

Figure 2-21 Plots of the total kinetic energy of an electron versus time without radiation reaction (solid curves) and with radiation reaction (dashed curves) for I_{peak} = 60 MA, r_l = 100 μm, τ_{pulse} = 100 ns, and electron emission at 5% peak current.

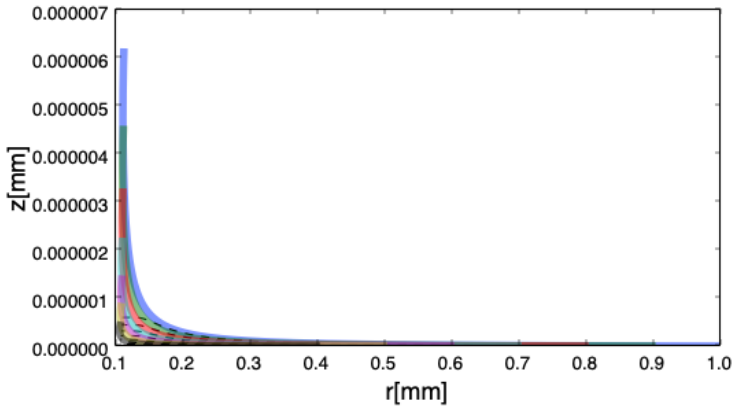

Figure 2-22 Plots of the electron guiding center motion without radiation reaction (solid curves) and with radiation reaction (dashed curves) for I_{peak} = 60 MA, r_l = 100 μm, τ_{pulse} = 100 ns, and electron emission at 5% peak current.

2.7. Summary of Significant Differences in Electron Simulations Due to Radiation Reaction

In this Section, we provide a summary of the significant differences between MITL electron simulations with or without radiation reaction physics. As we mentioned previously, the inclusion of radiation reaction physics causes significant changes in both the electron kinetic energy and its axial displacement. The following figures illustrate both of these effects as a function of peak MITL current. More specifically, the figures in Sections 2.2, 2.3, and 2.5 illustrate these differences for electrons at an initial radius $10 \times r_l$ with $r_l = 100\ \mu$m and $\tau_{pulse} = 100$ ns for the cases of 60 MA and 80 MA peak currents.

In Fig. 2-23, we see that the difference in peak kinetic energies with and without radiation reaction physics for the $10 \times r_l$ electron grows roughly linearly as a function of peak current. In this regard, the radiation reaction effect becomes increasingly important as the peak current increases. From a relative peak energy reduction standpoint, the difference is even more striking. Fig. 2-24 shows the percentage reduction in the peak kinetic energy when radiation reaction is enabled. It is clearly seen that some fraction of electrons will have approximately 90% peak kinetic energy reduction when radiation reaction is included compared to when it is not included. We should emphasize again that this reduction is due in part to the electrons radiated energy as well as its loss of magnetic moment that prevents it from gaining more kinetic energy at the load.

Since the electrons experience a loss of magnetic moment due to radiation reaction physics, the ∇B drift in the axial direction is also reduced. This can lead to mm-scale differences in the axial displacement of the electrons. Fig. 2-25, which plots the difference in the axial displacement for electrons at an initial radius $10 \times r_l$, illustrates this point clearly. For all NGPP current pulse lengths, we expect that some fraction of electrons will experience differences in axial displacement greater than 1 mm with and without radiation reaction physics near the load. As seen in Fig. 2-25, the absolute size of these differences can grow as a function of the peak current.

3. CONCLUSION

In this report, we have shown the results of electron simulations in radial NGPP MITLs with and without radiation reaction physics. We have found that radiation reaction physics becomes important when the magnetic fields that an electron experiences causes significant damping on time scales that are relevant to the MITL system. For MITL current pulse lengths of 100 ns and 200 ns, the relevant magnetic field strengths are B $>$ 7,200 T and B $>$ 5,100 T, respectively. These magnetic field strengths are readily achieved on a 60 MA NGPP MITL with load radii $<$ 1 mm. Hence, we expect that radiation reaction can be important in modeling electrons in NGPP MITLs near a 1 mm load.

We have found that the magnetic moment, which is a conserved quantity without radiation reaction physics, is significantly decreased when radiation reaction physics is enabled for all NGPP conditions that we studied. The reduction of the magnetic moment causes an immediate loss of cycloidal kinetic energy, but also prevents the electron from gaining more kinetic energy

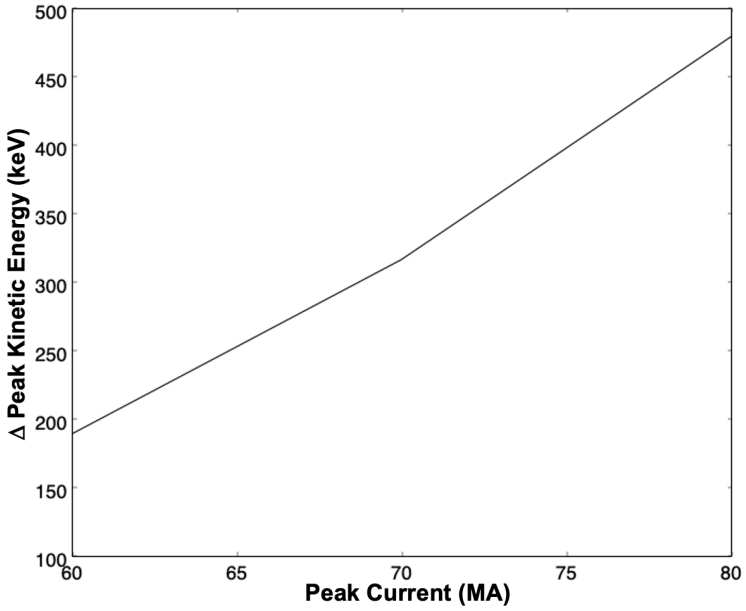

Figure 2-23 Plot of the difference in the peak kinetic energy for electrons at an initial radius 10 $\times$ r_l with r_l = 100 μm and τ_{pulse} = 100 ns.

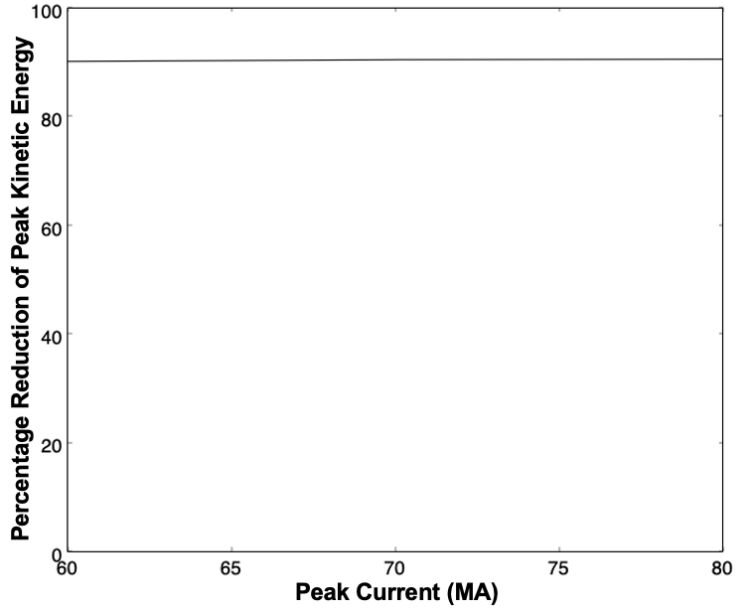

Figure 2-24 Plot of the percentage reduction of peak kinetic energy for electrons at an initial radius 10 $\times$ r_l with r_l = 100 μm and τ_{pulse} = 100 ns.

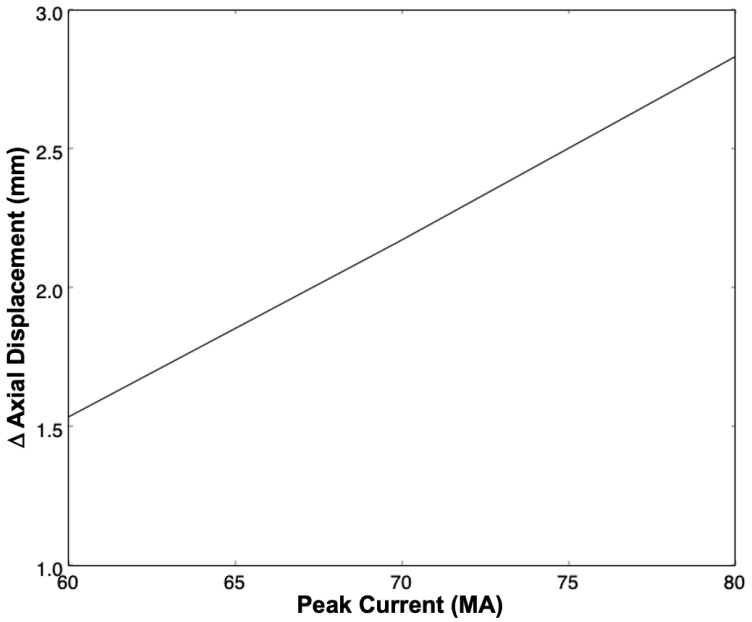

Figure 2-25 Plot of the difference in the axial displacement for electrons at an initial radius 10 $\times$ r_l with r_l = 100 μm and τ_{pulse} = 100 ns

as it radially drifts closer to the load. Additionally, the loss of magnetic moment causes a reduction of ∇B drift in the axial direction. Overall, the loss of magnetic moment can lead to significant differences in the electron's kinetic energy and axial displacement with and without radiation reaction enabled. The magnitude of these differences is directly related to the magnitude of the electron's initial magnetic moment.

We have shown that the difference in peak kinetic energy for electrons with or without radiation reaction is 100's of keV for electrons at 10 $\times$ r_l with r_l = 100 μm, τ_{pulse} = 100 ns and peak currents in the range of 60-80 MA. This reduction in the peak kinetic energy can be as much as 90% when radiation reaction is included. This reduction of electron kinetic energy in NGPP MITLs is a significant finding and warrants further investigation into the effects of radiation reaction physics in high-current power flow.

We should emphasize that the results of this study are based on a highly idealized single particle model with simplified electric and magnetic fields and no particle collisions. Future modeling of radiation reaction physics in power flow is needed to incorporate many particle physics, fully electromagnetic fields with space-charge physics, and collisional physics. Fully electromagnetic particle-in-cell codes that include radiation reaction physics are a possible tool for modeling this physics.

REFERENCES

[1] J. Larmor. LXIII. On the theory of the magnetic influence on spectra; and on the radiation from moving ions. *Philos. Mag*, 44:503, 1897.

[2] A. Liénard. Champ électrique et magnétique produit par une charge concentrée en un point et animée d'un mouvement quelconque. *L' Éclairage Électrique*, 16:5, 1898.

[3] H. A. Lorentz. Simplified Theory of Electrical and Optical Phenomena in Moving Systems. *Proceedings of the Royal Netherlands Academy of Arts and Sciences*, 1:427–442, 1899.

[4] M. Abraham. Prinzipien der Dynamik des Elektrons. *Physikalische Zeitschrift*, 4:57–62, 1902.

[5] P. A. M. Dirac. Classical theory of radiating electrons. *Proc. R. Soc. London*, A167:148, 1938.

[6] F. R. Elder, A. M. Gurewitsch, R. V. Langmuir, and H. C. Pollock. Radiation from electrons in a synchrotron. *Phys. Rev.*, 71:829–830, Jun 1947.

[7] J. Schwinger. On the Classical Radiation of Accelerated Electrons. *Phys. Rev.*, 75:1912–1925, Jun 1949.

[8] G. W. Ford and R. F. O'Connell. Relativistic form of radiation reaction. *Phys. Lett. A*, 174:182–184, 1993.

[9] J. D. Jackson. *Classical Electrodynamics*. John Wiley Sons, Inc., 1999.

[10] W. A. Stygar, T. J. Awe, J. E. Bailey, N. L. Bennett, E. W. Breden, E. M. Campbell, R. E. Clark, R. A. Cooper, M. E. Cuneo, J. B. Ennis, D. L. Fehl, T. C. Genoni, M. R. Gomez, G. W. Greiser, F. R. Gruner, M. C. Herrmann, B. T. Hutsel, C. A. Jennings, D. O. Jobe, B. M. Jones, M. C. Jones, P. A. Jones, P. F. Knapp, J. S. Lash, K. R. LeChien, J. J. Leckbee, R. J. Leeper, S. A. Lewis, F. W. Long, D. J. Lucero, E. A. Madrid, M. R. Martin, M. K. Matzen, M. G. Mazarakis, R. D. McBride, G. R. McKee, C. L. Miller, J. K. Moore, C. B. Mostrom, T. D. Mulville, K. J. Peterson, J. L. Porter, D. B. Reisman, G. A. Rochau, G. E. Rochau, D. V. Rose, D. C. Rovang, M. E. Savage, M. E. Sceiford, P. F. Schmit, R. F. Schneider, J. Schwarz, A. B. Sefkow, D. B. Sinars, S. A. Slutz, R. B. Spielman, B. S. Stoltzfus, C. Thoma, R. A. Vesey, P. E. Wakeland, D. R. Welch, M. L. Wisher, and J. R. Woodworth. Conceptual designs of two petawatt-class pulsed-power accelerators for high-energy-density-physics experiments. *Phys. Rev. ST Accel. Beams*, 18:110401, Nov 2015.

[11] R. J. Goldston and P. H. Rutherford. *Introduction to Plasma Physics*. Institute of Physics Publishing, 1995.

[12] M. H. Hess and E. G. Evstatiev. Electron dynamics within a MITL containing a load. *submitted to IEEE Trans. Plasma Sci.*, 2021.

[13] A. J. Brizard and A. A. Chan. Relativistic bounce-averaged quasilinear diffusion equation for low-frequency electromagnetic fluctuations. *Phys. Plasmas*, 2001.

[14] A.J. Brizard and T.S. Hahm. Foundations of nonlinear gyrokinetic theory. *Rev. Mod. Phys.*, 79(2):421–468, 2007.

[15] Robert G. Littlejohn. Variational principles of guiding centre motion. *J. Plasma Phys.*, 29(1):111–125, February 1983.

[16] Theodore G. Northrop. *The Adiabatic Motion of Charged Particles*. Interscience Publishers, 1963.

[17] M. Kruskal. The gyration of a charged particle. Technical Report NYO-7903; PM-S-33, Princeton Univ., N.J. Project Matterhorn, Mar 1958.

[18] Matthew R. Gomez, Stephen A. Slutz, Patrick F. Knapp, Kelly D. Hahn, Matthew R. Weis, Eric C. Harding, Matthias Geissel, Jeffrey R. Fein, Michael E. Glinsky, Stephanie B. Hansen, Adam J. Harvey-Thompson, Christopher A. Jennings, Ian C. Smith, Daniel Woodbury, David J. Ampleford, Thomas J. Awe, Gordon A. Chandler, Mark H. Hess, Derek C. Lamppa, Clayton E. Myers, Carlos L. Ruiz, Adam B. Sefkow, Jens Schwarz, David A. Yager-Elorriaga, Brent Jones, John L. Porter, Kyle J. Peterson, Ryan D. Mcbride, Gregory A. Rochau, and Daniel B. Sinars. Assessing stagnation conditions and identifying trends in magnetized liner inertial fusion. *IEEE Transactions on Plasma Science*, 47(5):2081–2101, 2019.

[19] M. S. Di Capua and D. G. Pellinen. Propagation of power pulses in magnetically insulated vacuum transmission lines. *J. Appl. Phys.*, 50:3713, 1979.

APPENDIX A. RADIATION REACTION FORCE IN A UNIFORM B-FIELD

In this Section, we derive the radiation reaction force and its effect on the kinetic energy of a charged particle in a uniform B-field, i.e. $\mathbf{B} = B\mathbf{e}_y$, given by Eq. (5). We assume that the particle has its velocity and momenta in all three directions, i.e. $\mathbf{v} = v_x\mathbf{e}_x + v_y\mathbf{e}_y + v_z\mathbf{e}_z$ and $\mathbf{p} = p_x\mathbf{e}_x + p_y\mathbf{e}_y + p_z\mathbf{e}_z$. The Lorentz force acting on the particle is given by $\mathbf{F} = q(\mathbf{v}\times\mathbf{B})$.

From the Lorentz force, we find that the parallel component of the momentum remains constant since it is unaffected by the magnetic field. However, since the motion of the particle perpendicular to the magnetic field is a circular orbit, the perpendicular momentum at time t can be derived from the momentum at $t = 0$, i.e. $\mathbf{p}_{0\perp}$, and is given by

$$\mathbf{p}_\perp = \mathbf{p}_{0\perp}\cos(\frac{qBt}{\gamma m}) + \mathbf{p}_{0\perp}\times\mathbf{e}_y\sin(\frac{qBt}{\gamma m}), \tag{28}$$

where $\gamma = \sqrt{1 + p_{0\perp}^2/m^2c^2 + p_\parallel^2/m^2c^2}$.

We can compute the radiation reaction force shown in Eq. (3) by taking time derivatives using Eq. (28). The first term on the right hand side of Eq. (3) is given by

$$\tau\gamma\frac{d\mathbf{F}}{dt} = \tau\frac{q}{m}\frac{d\mathbf{p}_\perp}{dt}\times\mathbf{B} = -\frac{\tau q^2B^2}{m^2\gamma}\mathbf{p}_\perp. \tag{29}$$

The second term can be decomposed into two parts, namely

$$-\frac{\tau\gamma^3}{c^2}\frac{d\mathbf{v}}{dt}\times(\mathbf{v}\times\mathbf{F}) = -\frac{\tau\gamma^3}{c^2}\frac{d\mathbf{v}}{dt}\times(\mathbf{v}_\parallel\times\mathbf{F} + \mathbf{v}_\perp\times\mathbf{F}). \tag{30}$$

The first term on the right hand side Eq. (30) yields a contribution to the radiation reaction force which is in the direction of the parallel momentum, i.e.

$$-\frac{\tau\gamma^3}{c^2}\frac{d\mathbf{v}}{dt}\times(\mathbf{v}_\parallel\times\mathbf{F}) = -\frac{\tau q^2B^2}{m^2}\frac{\gamma v_\perp^2}{c^2}\mathbf{p}_\parallel. \tag{31}$$

Conversely, the second term on the right hand side Eq. (30) yields a contribution to the radiation reaction force which is in the direction of the perpendicular momentum, i.e.

$$-\frac{\tau\gamma^3}{c^2}\frac{d\mathbf{v}}{dt}\times(\mathbf{v}_\perp\times\mathbf{F}) = -\frac{\tau q^2B^2}{m^2}\frac{\gamma v_\perp^2}{c^2}\mathbf{p}_\perp. \tag{32}$$

Combining Eqs. (29), (31), and (32) yields the force shown in Eq. (5), i.e.

$$\mathbf{F}_{rad} = -\frac{\gamma v_\perp^2/c^2\mathbf{p}_\parallel}{\tau_{damp}} - \frac{\gamma(1 - v_\parallel^2/c^2)\mathbf{p}_\perp}{\tau_{damp}}. \tag{33}$$

In order to complete the calculation for the case of a uniform B-field, we look at the kinetic energy loss due to the radiation reaction force. The kinetic energy of the particle is given by $K = (\gamma - 1)mc^2$. The rate of total kinetic energy loss is given by

$$\frac{dK}{dt} = \frac{d\gamma}{dt}mc^2 = \frac{1}{\gamma m}\mathbf{p}\cdot\frac{d\mathbf{p}}{dt} = \frac{1}{\gamma m}\mathbf{p}\cdot\mathbf{F}_{rad}. \tag{34}$$

Using Eq. (33), we find that the rate of total kinetic energy due to the radiation reaction force is given by

$$\frac{dK}{dt} = -\frac{(c^2 - \mathrm{v}_\parallel^2)p_\perp^2 + \mathrm{v}_\perp^2 p_\parallel^2}{m\tau_{damp}c^2} = -\frac{p_\perp^2}{m\tau_{damp}}. \tag{35}$$

As shown in Eq. (35), the reduction of energy loss in the perpendicular direction due to the presence of the parallel momentum is offset by energy loss in the parallel direction which is coupled to the perpendicular momentum. Moreover, although the radiation force affects the parallel and perpendicular components of the momentum as shown in Eq. (33), the total kinetic energy loss of the particle only depends on the magnitude of the perpendicular momentum.

DISTRIBUTION

Email—Internal [redacted]

Name	Org.	Sandia Email Address
Mark Hess	1684	mhess@sandia.gov
Evstati Evstatiev	1684	egevsta@sandia.gov
Kristian Beckwith	1684	kbeckwi@sandia.gov
Kyle Peterson	1601	kpeters@sandia.gov
Technical Library	1911	sanddocs@sandia.gov

Sandia National Laboratories

Sandia National Laboratories is a multimission laboratory managed and operated by National Technology & Engineering Solutions of Sandia LLC, a wholly owned subsidiary of Honeywell International Inc., for the U.S. Department of Energy's National Nuclear Security Administration under contract DE-NA0003525.